RSC Advances

PAPER

View Article Online
View Journal | View Issue

Cite this: *RSC Adv.*, 2022, **12**, 34746

Insights into chalcone analogues with potential as antioxidant additives in diesel–biodiesel blends†

Igor D. Borges, *[ab] Eduardo C. M. Faria, [ab] Jean F. M. Custódio, [a] Vitor S. Duarte,[ab] Fernanda S. Fernandes,[c] Christian G. Alonso, [c] Flávio O. Sanches-Neto, [ad] Valter H. Carvalho-Silva, [a] Guilherme R. Oliveira[c] and Hamilton B. Napolitano *[a]

Received 17th November 2022
Accepted 17th November 2022

DOI: 10.1039/d2ra07300e

rsc.li/rsc-advances

Biodiesel production is one of the promising strategies to reduce diesel consumption and an important contribution to climate change. However, biodiesel stability remains a challenging problem in biofuel use in the global energy matrix. In this context, organic additives have been investigated to minimize these problems and reduce harmful emissions to comply with fuel requirement standards. In this study, we discuss a comprehensive structural description, a behavior of B15 [85% volume of diesel and 15% volume of biodiesel (B100)] stability in the presence of antioxidants (chalcone analogues), and a theoretical calculation to pave the way for clarifying and expanding the potential of title compounds as an antioxidant additive for diesel–biodiesel blends. Finally, a systematic description of the oxidation stability was undertaken using a specialized machine learning computational pySIRC platform.

1. Introduction

Recently, anthropogenic environmental impacts have been under discussion focused on the world, promoting changes in different societal sectors.[1,2] From the energetic scope, new policies have restricted the fossil fuels use that will gradually be replaced by renewable energy matrices, which are more sustainable and generate lower levels of pollutant emissions.[3–6] The United Nations Conference on Climate Change (COP26)[7] has discussed issues such as reducing pollution emissions and dependence on fossil fuels through the use of renewable energy.[8,9] Countries have also made commitments to step up and phase out coal, end international financing for fossil fuels, 50% reduction in greenhouse gas emissions by 2030, and among other objectives, pave the pathway for a net-zero emission future.[10–13]

The use of biodiesel from biomass feedstocks is recognized as a sustainable option and advocated due to the serious global environmental security challenges.[14–16] The properties of biodiesel are similar to those of petro-diesel with significant benefits, including being non-toxic, having a higher flash point (423 K for biodiesel as compared to 337 K for petro-diesel)[14] and noteworthily lower pollutant emissions and particulate matter.[17–19] However, the full adoption of biofuels is hampered by the fact that they are more susceptible to oxidation than mineral diesel.[17,19–21] The reduction of the blend's shelf-life, when used after long storage periods, can damage mechanical elements in the engine, reduce efficiency, and have the potential to give rise to harmful emissions.[17–20,22,23] The degradation rate is considered one of the most important parameters to evaluate the shelf-life of the blend during its storage, where a low value of rate constant indicates greater oxidative stability.[24,25]

Generally, biodiesel filled with natural or synthetic antioxidant additives can decrease the rate of degradation reactions in biodiesel.[17,21,26] The additives when associated with biodiesel fractions are a gimmick to mitigate nitrogen oxide (NO_x) emissions from the fuel combustion in diesel engines.[17–19,27] The development of chemical additives whose properties favor better storage stability for biodiesel and its blends with diesel is needed. Previous studies have shown that the addition of chalcone compounds into diesel–biodiesel blends reduces the rate of the oxidation process.[28,29] This class of flavonoid intermediates is formed by two aromatic rings linked by a three-carbon bridge having a keto carbonyl group and one α,β-unsaturation, obtained from natural sources[30–32] or synthetic pathways.[33,34] Some physicochemical properties, such as antibacterial,[35–37] antifungal,[38–40] and antioxidant,[28,41] are the key issue for their ability to prevent free radical-induced oxidative damage driven by substitutions in chalcone rings as a function of their chemical flexibility.[42–47]

In light of these facts, and as part of our ongoing work regarding the application of chalcones as antioxidant biodiesel

[a]*Grupo de Química Teórica e Estrutural de Anápolis, Universidade Estadual de Goiás, Anápolis, GO, Brazil. E-mail: hamilton@ueg.br; i.dalarmelino@gmail.com; Tel: +55 (62) 3328-1156*

[b]*Centro de Pesquisa e Eficiência Energética, CAOA Montadora de Veículos LTDA, Anápolis, GO, Brazil*

[c]*Instituto de Química, Universidade Federal de Goiás, Goiânia, GO, Brazil*

[d]*Instituto de Química, Universidade de Brasília, Brasília, DF, Brazil*

† Electronic supplementary information (ESI) available. CCDC 2182574 and 2182577. For ESI and crystallographic data in CIF or other electronic format see DOI: https://doi.org/10.1039/d2ra07300e

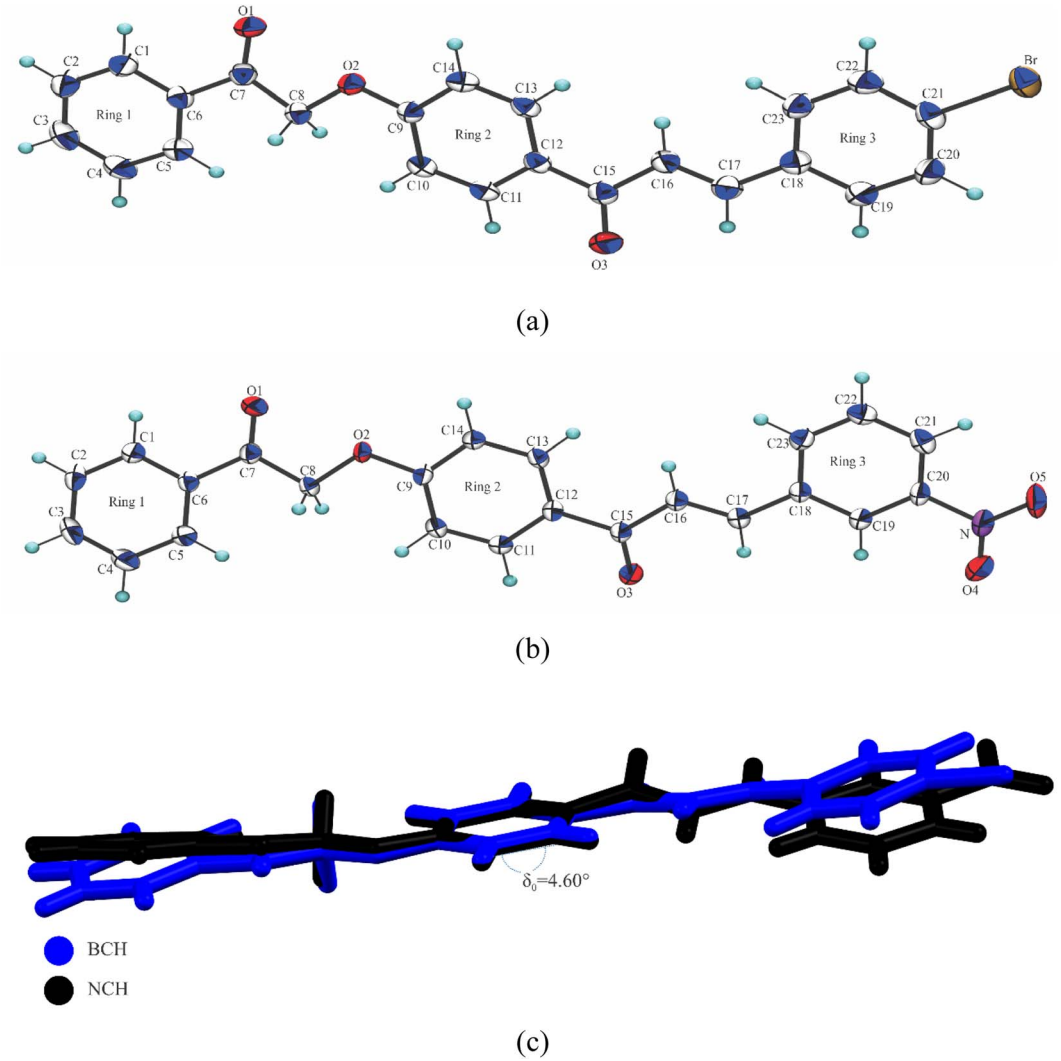

Fig. 1 The ORTEP diagram for BCH (a) and NCH (b). The ellipsoids are represented at a 75% probability level with the atomic numbering scheme. Hydrogen atoms are represented by spheres with arbitrary radii. Structure overlay for BCH and NCH $\delta_0 = 4.60°$ (c).

additives,[28,29,48] in this paper, we discuss the synthesis, extensive structure characterization, oxidation stability test, and density functional theory (DFT)[49] calculations for (2*E*)-3-(4-bromophenyl)-1-[4-(2-oxo-2-phenylethoxy)phenyl]prop-2-en-1-one (BCH) and (2*E*)-3-(3-nitrophenyl)-1-[4-(2-oxo-2-phenylethoxy)phenyl]prop-2-en-1-one (NCH) (see structures in Fig. 1). Because fundamental thermodynamic parameters are stimulated by changing aromatic ring substitutions[50–52] we hypothesized that BCH and NCH, in terms of biodiesel feedstock,[17,19,53] could be investigated as an additive for diesel–biodiesel blends. An explanation of the kinetic factors involved in oxidation stability was assessed using a machine-learning computational platform.

2. Experimental and computational procedures

2.1. Synthesis and spectroscopy characterization

1.2 mL of K_2CO_3 (0.2 mmol) was added to the solution of hydroxychalcone (0.1 mmol) in acetone and the system cooled to 0 °C. Subsequently, phenacyl bromide (0.14 mmol) was added in a single portion, and the mixture was stirred at room temperature for 2 h. The reaction was monitored by thin-layer chromatography (TLC) and quenched with distilled water (1.2 mL), and the product was extracted with CH_2Cl_2 (3 × 10 mL). The synthesis was carried out with specific chemical elements (hydroxychalcone, K_2CO_3, phenacyl bromide, CH_2Cl_2, anhydrous Na_2SO_4, and methanol) that were purchased from companies specialized in the sale of chemical reagents.[54] BCH ^{1}H NMR (500 MHz, $CDCl_3$): 5.39 (s, 1H); 7.02 (m, 2H); 7.49 (m, 7H); 7.66 (m, 1H); 7.71 (d, 1H, J = 15.7 Hz); 8.02 (m, 4H). ^{13}C NMR (125 MHz, $CDCl_3$): 70.5; 114.4; 114.6; 122.3; 124.6; 128.1; 129.0; 129.7; 130.8; 132.2; 134.2; 142.8; 161.8; 188.4. NCH ^{1}H NMR (500 MHz, $CDCl_3$): 5.41 (s, 1H); 7.05 (m, 2H); 7.54 (m, 2H); 7.60 (d, 1H, J = 15.9 Hz); 7.66 (m, 2H); 7.81 (d, 1H, 15.7 Hz); 7.91 (m, 1H); 8.02 (m, 2H); 8.06 (m, 2H); 8.25 (m, 1H); 8.51 (m, 1H). ^{13}C NMR (125 MHz, $CDCl_3$): 70.5; 114.8; 122.2; 124.5; 128.1; 129.0; 130.2; 131.0; 131.3; 131.7; 134.2; 141.0; 145.8; 162.1; 187.8; 193.4.

2.2. Crystallographic analysis

The organic phase was dried with anhydrous Na_2SO_4, filtered, and concentrated in a vacuum. After recrystallization by slow evaporation of methanol, the product was obtained as a yellow crystalline solid with a 34% yield. The X-ray diffraction data were obtained using a Bruker APEX II CCD diffractometer fitted with MoKα radiation ($\lambda = 0.71073$ Å) at room temperature. The structure was solved on SHELXT[55] and refined on SHELXL[56] using the OLEX2 (ref. 57) platform. The non-hydrogen atoms were refined anisotropically. The hydrogen atoms were refined using the riding model with the individual isotropic displacement parameters or $U_{iso}(H) = 1.2U_{eq}$ of the bonded carbon. All supramolecular representations were generated using mercury[58] and molecular interactions were checked using PLATON.[59] The crystallographic information files were deposited at the Cambridge Crystallographic Data Centre (CCDC)[60] under codes 2182574 and 2182577.

The hirshfeld surface (HS) describes intermolecular interactions through color-scaled mapping (red, white, and blue) that permits the identification and description of surface properties.[52] Where red indicates regions with short intermolecular contacts, white indicates contacts around the separation of the van der Waals radii interface, and blue indicates long contact distances.[52] The three-dimensional graph of the HS, the d_{norm} (normalized distance), was constructed by the surface distance to the closest exterior atom (d_e), where the molecules act as the strongest intermolecular contact receptors, by the surface distance to the closest interior atom (d_i), where the molecule acts as the strongest intermolecular donor contact, with the van der Waals radius (r_i^{vdW} and r_e^{vdW}) for each atom involved in this close contact with the surface:[61]

$$d_{norm} = \frac{d_i - r_i^{vdW}}{r_i^{vdW}} + \frac{d_e - r_e^{vdW}}{r_e^{vdW}} \quad (1)$$

The complementarity between molecules in the crystal packing, hydrophobic intermolecular interactions, and interactions involving the π system ($\pi \ldots \pi$ interactions), was identified from the shape index surface.[61] In addition, the combination of d_e and d_i, generate unique fingerprints for each molecule in the form of 2D plots, allowing a quantitative analysis of each type of intermolecular contact.[61]

2.3. Storage stability test

The storage stability of S10 diesel containing a 15% volume of biodiesel (S10 B15 diesel) was verified. The S10 B15 diesel was composed of 85% volume of biodiesel-free reference diesel (fuel according to RANP 764/2018,[62] applied on emission and consumption tests) and 15% volume of biodiesel (B100) (composed of 60% volume of soybean oil, 37% volume of palm oil, 2% volume of bovine fat and 1% volume of pig fat). Thus, high-density polyethylene (HDPE) bottles of 1 liter capacity were filled with 300 mL of each sample: bottle 1 – diesel S10 B15 containing 109.0 ppm of the BCH, bottle 2 – diesel S10 B15 containing 100.7 ppm of NCH and bottle 3 – diesel S10 B15 without additive. The three flasks remained in an external environment for 90 days. After this period, the oxidation stability was measured using the modified Rancimat method according to the EN 15751:14 standard.[63]

2.4. Oxidation stability test

The modified Rancimat test method is an important experiment applied to verify diesel–biodiesel blend oxidation stability. It is a standard procedure for the storage stability certification of diesel cycle engine fuels. In the Rancimat test, the sample was heated to 110 °C and subjected to a purified airflow to supply oxygen (induction period process). Thus, oxygen promotes oxidation reactions in the sample, forming peroxides as products, which, due to the high temperature, are dissociated and form volatile compounds such as aldehydes, ketones, and carboxylic acids. These compounds are directed to a container filled with deionized water, which is coupled to a conductivity electrode, and are detected when the conductivity increases quickly, indicating high ion concentrations and the end of the test. The induction period is reported as hours. Therefore, the longer the induction period, the greater the oxidation stability of the sample.[64,65] For our analysis, Metrohm 873 model equipment was applied according to EN 15751: 2014 test method.[63]

2.5. Computational procedures

The theoretical analysis for both chalcones was performed using DFT.[49] The geometric parameters obtained from the X-ray data were optimized in the gas phase, with theoretical calculations carried out in the Gaussian09 (ref. 66) software, using M06-2X/6-311++G(d,p),[67–69] From the generated wave function, Frontier molecular orbitals were calculated, (highest occupied molecular orbital (HOMO) and lowest unoccupied molecular orbital (LUMO).[50,51] To investigate the reactive sites of both chalcones, the MEP map was constructed from the equation:

$$V(r) = \sum_{\alpha} \frac{Z_A}{|r_\alpha - r_A|} - \int \frac{\rho®}{r_\alpha - r} dr \quad (2)$$

where® (r) is a potential created at a point r, the first term of summation is the electrostatic potential created by the nucleus and the second term is the electrostatic potential created by electrons.[70]

To identify the main oxidation sites of BCH and NCH, appropriate local reactivity descriptors, such as Fukui function (f),[71,72] were calculated according to equations $f_{NBO}{}^{+} \approx \rho_{NBO}^{HOMO} = \sum_i |c_i|^2_{HOMO}$, $f_{NBO}{}^{-} \approx \rho_{NBO}^{LUMO} = \sum_i |c_i|^2_{LUMO}$, and $f_{NBO} \approx f_{NBO}{}^{+} + f_{NBO}{}^{-}/2$. The Multiwfn package program[73] was used to study the topological and Fukui functions. The oxidation reactions promoted by oxygen supply were simulated by pySIRC[74] – a machine learning computational platform. The hydroxyl radical – an archetypal system of degradation reactions – was selected to mimic the oxidation effect promoted using the oxygenation process.

3. Results and discussion

3.1. Solid-state description

BCH and NCH crystallize in the $P\bar{1}$ and the $P2_1$ space groups, respectively. Table 1 summarizes the structure refinement parameters, and the ORTEP[75] representation is shown in Fig. 1. Structural differences between the two compounds occur in the ligands of aromatic ring 3. A bromine atom in BCH is bonded an *ortho* carbon (C_{21}), and a hydrogen atom is bonded to the *meta* carbon (C_{20}). On the other hand, in NCH the ligand in position *ortho* is a hydrogen atom, while a nitro group is bound to the *meta* carbon (C_{20}).

Bond lengths (Table S1†) of BCH and NCH of carbon–carbon and carbon-oxygen were very close to each other for the chalcones. The largest variations occurred for O_2–C_9 (0.0084 Å), C_{21}–C_{22} (0.0079 Å), C_6–C_7 (0.0063 Å), and C_2–C_3 (0.0058 Å). In turn, bond angles (Table S2†) calculated for the BCH and NCH present the largest variations in C_{20}–C_{21}–C_{22} (4.07°), C_{21}–C_{20}–C_{19} (4.73°), C_{18}–C_{19}–C_{20} (2.51°), where the angles in parentheses represent the calculated difference between BCH and NCH for each bonded trio atoms. The angular variations occurred because of the different compounds attached to aromatic ring 3 for each chalcone, affecting the angular positions of C_{18}, C_{19}, C_{20}, C_{21}, and C_{22} atoms, which together with carbon 23, form the aromatic ring 3. BCH (Fig. S1a†) is almost planar and displays an angle between aromatic rings 1 and 2 $\delta_1 = 6.75°$.

A major deviation from planarity was found between aromatic rings 2 and 3, with a plan angle of $\delta_2 = 13.03°$. In NCH, however (Fig. S1b†), the interplanar angles are $\delta_3 = 9.24°$ (between rings 1 and 2) $\delta_4 = 6.62°$ (between rings 2 and 3) and the largest deviation from planarity is $\delta_5 = 21.83°$ (between rings 1 and 3). The superposition of the chalcones (Fig. 1c) allows the comparison between the geometric parameters of the structures. The root means squared (RMS) value predicted by

Table 1 Crystal data and structure refinement for BCH and NCH

Parameter	BCH	NCH
Empirical formula	$C_{23}H_{17}BrO_3$	$C_{23}H_{17}NO_5$
Formula weight	421.27	387.38
Temperature K^{-1}	120.02	120
Crystal system	Triclinic	Monoclinic
Space group	$P\bar{1}$	$P2_1/n$
a/Å	6.6262(3)	7.3047(12)
b/Å	7.4872(4)	11.062(2)
c/Å	19.2803(10)	22.299(4)
α/°	87.424(2)	90
β/°	87.609(2)	98.363(3)
γ/°	71.455(2)	90
Volume/Å^3	905.56(8)	1782.7(6)
Z	2	4
ρ_{calc} g cm^{-3}	1.545	1.443
μ/mm^{-1}	2.291	0.103
F(000)	428	808
Crystal size mm^{-3}	0.316 × 0.177 × 0.024	0.618 × 0.123 × 0.109
Radiation	MoKα ($\lambda = 0.71073$)	MoKα ($\lambda = 0.71073$)
2Θ range for data collection/°	4.232 to 56.422	3.692 to 56.558
Index ranges	$-8 \le h \le 8$, $-9 \le k \le 9$, $-25 \le l \le 25$	$-9 \le h \le 9$, $-14 \le k \le 14$, $-29 \le l \le 29$
Reflections collected	10 681	25 512
Independent reflections	4424 [$R_{int} = 0.0254$, $R_{sigma} = 0.0355$]	4432 [$R_{int} = 0.0288$, $R_{sigma} = 0.0197$]
Data/restraints/parameters	4424/0/244	4432/0/262
Goodness-of-fit on F^2	1.011	1.019
Final R indexes [$I \ge 2\sigma$ (I)]	$R_1 = 0.0327$, w$R_2 = 0.0705$	$R_1 = 0.0373$, w$R_2 = 0.0981$
Final R indexes [all data]	$R_1 = 0.0447$, w$R_2 = 0.0746$	$R_1 = 0.0509$, w$R_2 = 0.1058$
Largest diff. peak/hole/e Å^{-3}	0.43/−0.36	0.39/−0.23

Table 2 Hydrogen-bond geometry obtained from structural analysis for BCH and NCH

	D–H … A	D–H (Å)	H … A (Å)	D … A (Å)	D–H … A (°)	Symmetry code
BCH	C_3–H_3…Br	0.95(1)	2.92(3)	3.867(2)	173(4)	$-2 + x, 1 + y, 1 + z$
	C_4–H_4…O_1	0.95(1)	2.54(5)	3.166(3)	123(6)	$-1 + x,y,z$
	C_{13}–H_{13}…O_1	0.95(1)	2.703(4)	3.494(3)	141(5)	$1 - x, 2 - y, 1 - z$
NCH	C_5–H_5…O_4	0.95(1)	2.62(5)	3.363(1)	134(4)	$1 - x, 1 - y,1 - z$
	C_{22}–H_{22}…O_2	0.95(1)	2.56(6)	3.456(16)	157(6)	$1 - x, 2 - y, 1 - z$
	C_{22}–H_{22}…O_1	0.95(1)	2.64(4)	3.254(2)	122(6)	$1 - x, 2 - y, 1 - z$
	C_{13}–H_{13}…O_1	0.95(1)	2.63(3)	3.463(2)	145(4)	$-x, 2 - y, 1 - z$
	C_2–H_2…O_5	0.95(1)	2.47(4)	3.2077(16)	135(3)	$-5/2 + x,3/2 - y,1/2 + z$

the mercury program package is 0.0194 Å. Changing the substituent on aromatic ring 3 promotes a significant improvement in the planarity, since the planarity in the chalcones is related to donor–acceptor interactions in a molecule, on position and the vicinity of the substituents.[76–78] Chalcones have structures that are generally identified with almost planar conformation, a conformational requirement that may be related to their potential for antifungal activity.[78–82] This activity is necessary to maintain the quality of fuels since the proliferation of microorganisms is harmful to the system.[83,84]

Crystal engineering seeks to explore the multiplicity of intermolecular interactions in a crystalline environment. HS analysis allows the location of crucial contacts on the packaging, dependent on molecular geometry, locations, and orientation of the neighbouring molecules. The interactions listed in Table 2 were confirmed by electron density HS mapped

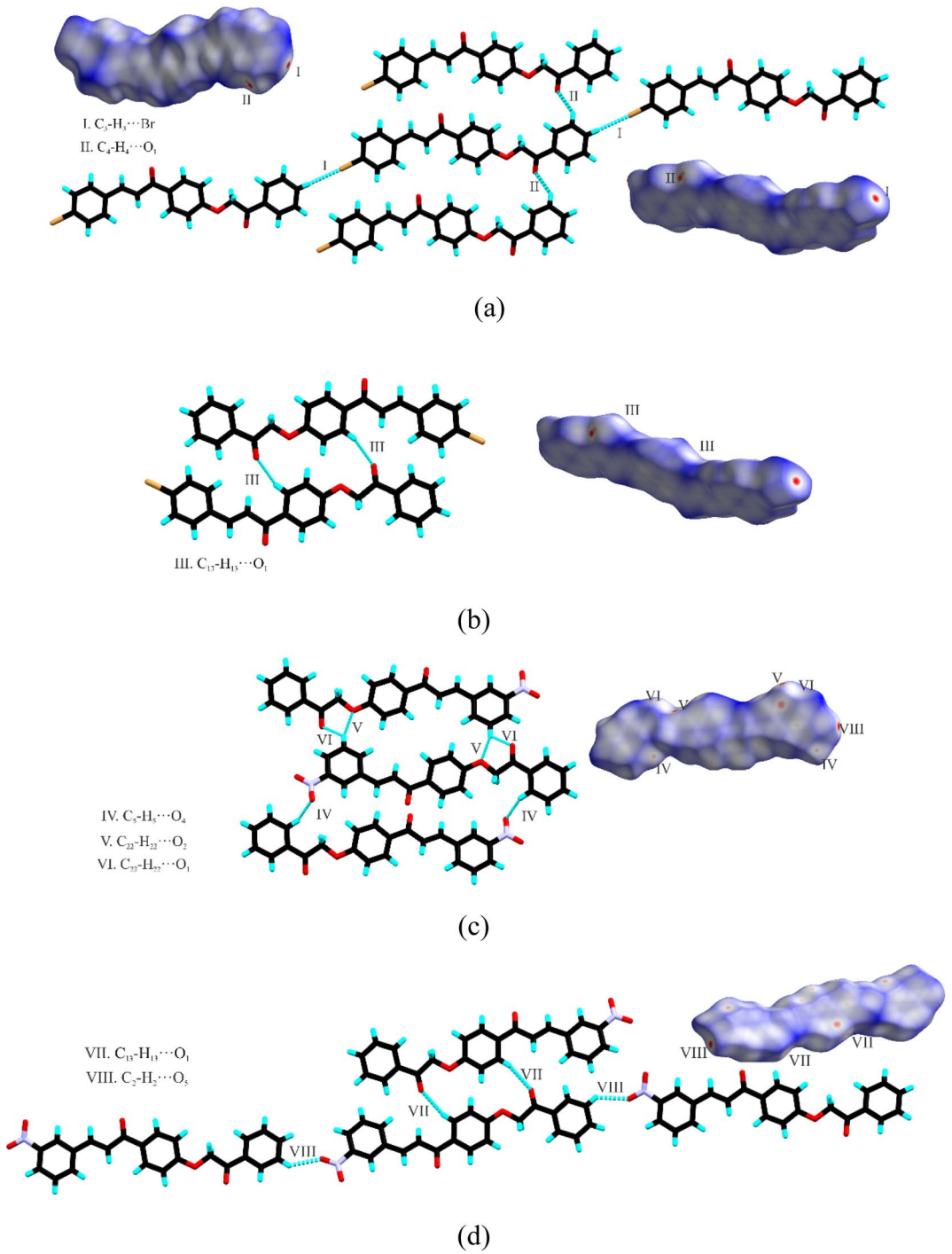

Fig. 2 The representation of interactions and HS d_{norm} showing the contacts for BCH (a) C_3–H_3…Br(I) C_4–H_4…O_1(II) and (b) C_{13}–H_{13}…O_1 (III). The NCH (c) C_5–H_5…O_4 (IV), C_{22}–H_{22}…O_2 (V) and C_{22}–H_{22}···O_1 (VI) and (d) C_{13}–H_{13}…O_1 (VII) and C_2–H_2…O_5 (VIII).

over d_{norm} (ranging from −0.1019 to 1.3604 BCH and −0.1685 to 1.4111 NCH). The supramolecular arrangement of BCH (Fig. 2a and b) is stabilized by the C_3–H_3…Br interaction contributing to the direction [001] described as $C_1^1(20)$ and weak interactions C_4–H_4…O_1, involving aromatic hydrogen since the most significant hydrogen bond motif is $C_1^1(6)$ and $R_2^2(16)$ C_{13}–H_{13}…O_1 forming a dimer with periodicity along [100] in a bifurcated fashion. In contrast, the supramolecular structure of NCH crystal (Fig. 2c and d) has three dimers and a bifurcated interaction along the [010] direction, C_5–H_5…O_4 (IV) C_{22}–H_{22}…O_2 (V)C_{22}–H_{22}…O_1 (VI), C_{13}–H_{13}…O_1 (VII) with motifs $C_1^1(19)$, $R_2^2(24)$, $R_2^2(30)$ and $R_2^2(16)$ respectively, and C_2–H_2…O_5 contributing to the [100] direction.

The π…π stacking is a type of non-covalent interaction, represented by the red and blue triangles (bow tie), and contributes to the stability of structures. For this interaction, the centroid of the aromatic rings for the compounds was calculated, with the distance between the two rings. The distance between the centroids, formed between the center of the aromatic rings is $d_1 = 3.746$ Å and $d_2 = 3.729$ Å for BCH (Fig. 3a) and $d_3 = 3.802$ Å $d_4 = 3.709$ Å and $d_5 = 3.725$ Å for NCH (Fig. 3b). The introduction of nitro group atoms into the structure caused a decrease in the stacking distance π…π.

The relative surface area resulting from the contributions of the interactions exposed in the crystal is quantified by analysing the fingerprint (Fig. 4), generated from the d_e *vs.* d_i plot. The graph represents a bin formed by intervals (0.2 Å). These can be decomposed into contributions of specific atoms, which makes it possible to measure the relative importance of several contacts when comparing the structure. Most of the contacts are H···H, which represents 38.2% of the HS for BCH and 35.2% for NCH, characterized by the central peak of the graph. O··· H interactions are characterized by the small peaks at the bottom of the fingerprint, representing 16.4% for BCH and 31.6% for NCH. The high difference is explained by the presence of the nitro group and the competition caused by the bromine atom in BCH shown by the peaks at the side edge of the graph. Also, we can ascertain that for NCH the most and strongest hydrogen bonds are present. Furthermore, the C··· C contacts with 12.1% for BCH and 13.0% NCH, present in the center, which helps in understanding π···π interaction. The interlayer contacts of C···O show weak interactions (distances above 3.5 Å) and therefore can be neglected.

3.2. Antioxidant additive analysis

The shelf-life tests evaluated the performance of BCH and NCH chalcones as antioxidant additives for diesel–biodiesel blends during storage of 90 days. Brazilian legislation does not specify the minimum oxidation stability for the commercial diesel-biodiesel blend. However, the resolution ANP 798/2019(ref. 85) determines a minimum limit of oxidation stability at 110 ° C for commercial biodiesel (B100): a minimum of 12 hours, measured according to EN 15751: 2014 test method.[63] However, European regulations include the specification of oxidation stability for the diesel–biodiesel blend BS EN 590:2009,[86] which establishes requirements and test methods for automotive fuels used in diesel cycle engines. As such, the result of the induction period shall be higher than 20 hours for the fuel to be considered suitable for use.

During the sample preparation at the test start, chalcone concentrations added to the flasks differed by 8.3 ppm. Converting this change-over to mol quantity/volume unity, this variation is less significant, on the order of 1.2×10^{-9} mol.mL^{-1}. Therefore, the chalcones' content was very similar in these two cases. The results shown in Table 3 indicate the oxidation stability values above 30 hours for two types of mixtures (containing BCH e NCH), both results above the induction period of biodiesel without additives that were subjected to the same stability test conditions. The average oxidation stability obtained for the fuel containing the NCH was 2.3% higher than that for the fuel with BCH. Joshi *et al.* (2013)[87] showed that the additive concentrations (300, 400, and 500

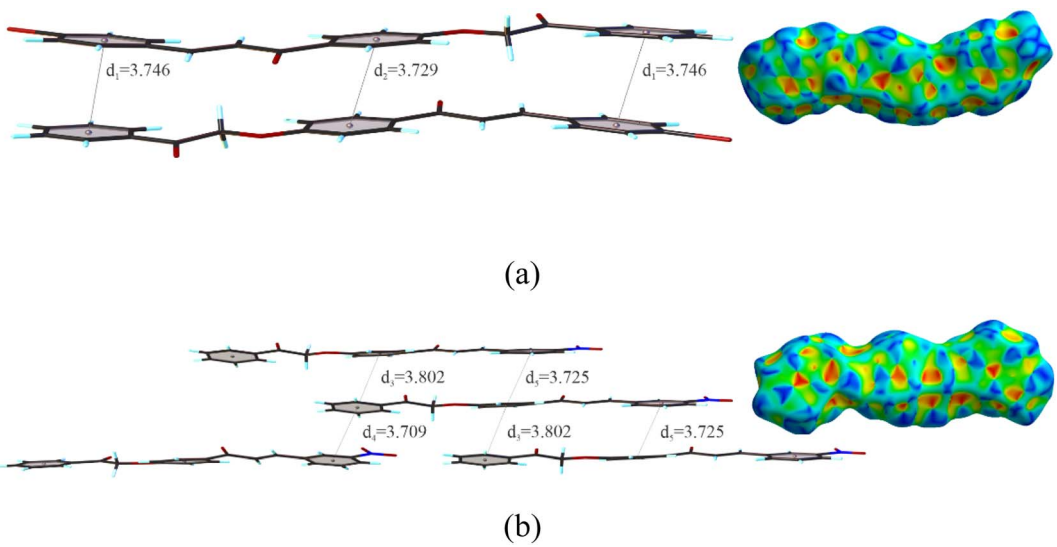

Fig. 3 . Shape index surfaces for evidencing π…π interactions and representation of BCH (a) and NCH (b).

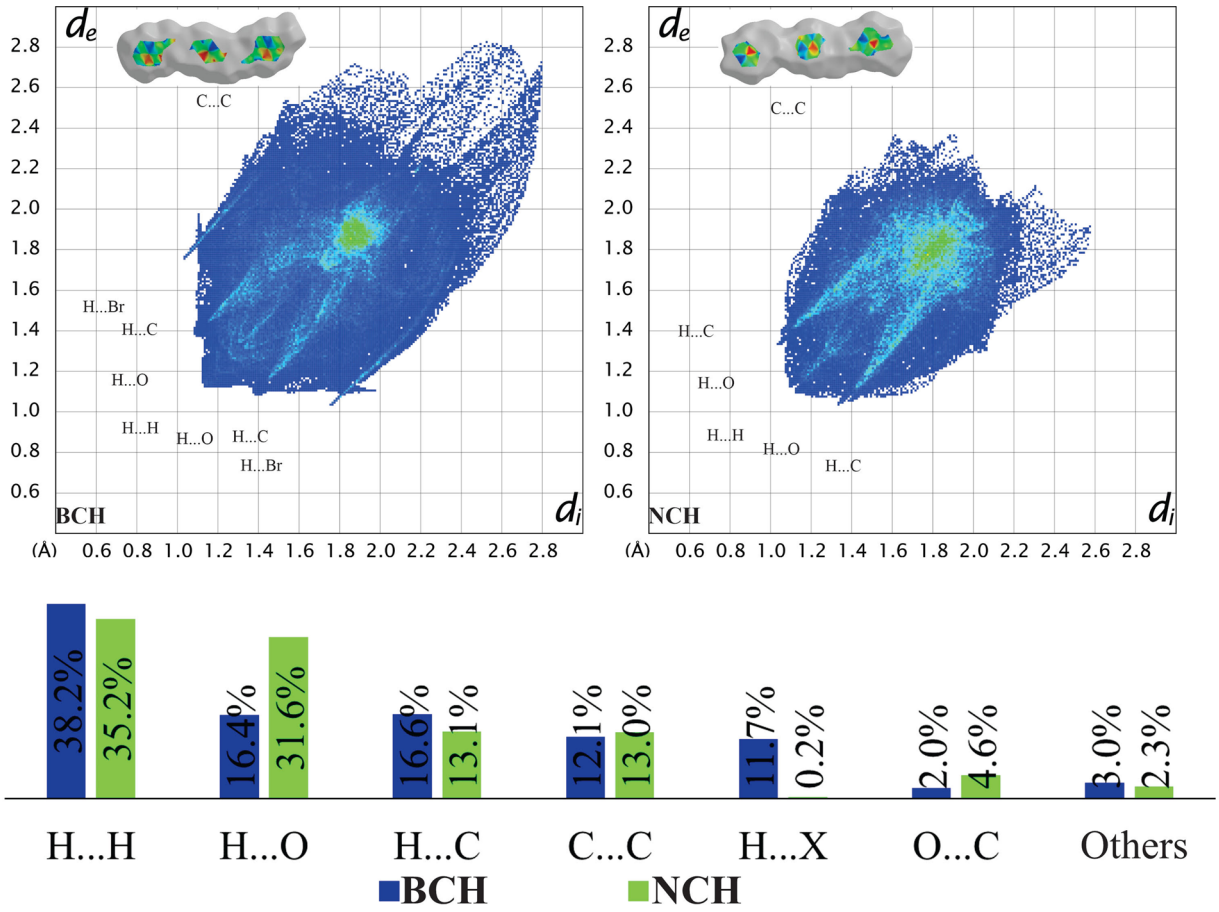

Fig. 4 Fingerprint plots with quantitative analysis of the contacts for BCH and NCH (where X = Br and N).

Table 3 Oxidation stability results from the modified Rancimat method

Modified Rancimat	Result 1	Result 2	Result 3	Average	Standard deviation
S10 B15 + BCH (109.0 ppm)	32.15 h	31.27 h	30.73 h	31.38 h	0.585
S10 B15 + NCH (100.7 ppm)	32.78 h	32.00 h	31.51 h	32.10 h	0.523
S10 B15 without additives	31.21 h	31.23 h	30.78 h	31.07 h	0.208

ppm) are correlated with the stability; the additives butylated hydroxy anisole (BHA), butylated hydroxytoluene (BHT), pyrogallol (PY), propyl gallate (PG), *tert*-butylhydroxyquinone (TBHQ), and diphenylamine (DPA) showed the values under 30 h to B15 blend. Also, Rizwanul *et al.* (2014)[88] showed the following oxidative stability values for the high concentration of additives (2000 ppm) to the B20 blend: TBHQ (28.38 h) > BHT (25.28 h) > BHA (22.27 h). Agarwal *et al.* (2015)[89] showed the following values for 500 ppm concentration of additives on pure biodiesel (B100): BHT (5 h), BHA (6 h), TBHQ (4), PG (15 h) and PY (25 h). Moreover, the linear correlation between the antioxidant concentration and the induction period was observed,[17,90–92] which could allow assessing the minimum additive concentrations to their respective effectiveness. The use of chalcone analogues is promising in retaining the biodiesel physicochemical properties during the oxidative processes – especially at low concentrations (typically 200–2000 ppm).[17,92]

The modified Rancimat (EN 15751: 2014 test method)[63] defines the repeatability factor (r) applied to results obtained by the same operator with the same apparatus under constant operating conditions. It is determined from eqn (3) with a confidence level of 95%, in which x is the three average results (Table 3):

$$r = 0.22027 + 0.04344x \quad (3)$$

The uncertainties were estimated from the repeatability factor, and they are registered in Fig. 5, both equal to approximately ± 1.6 h.

According to Karavalakis *et al.* (2009)[93] fuel aging can be accelerated in the presence of heat, oxygen, water, metal ions,

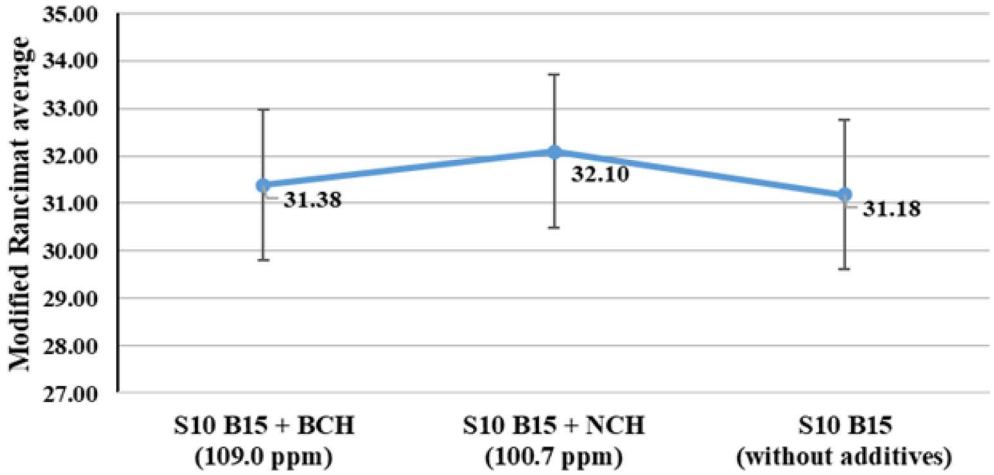

Fig. 5 The measurement uncertainty estimate of oxidation stability results from the modified Rancimat method.

and other impurities, favoring a viscosity increase due to gum and residue formation.[94] During the oxidation process of diesel–biodiesel blends, there is also a reduction in the flash point because of aldehyde formation, as well as an increase in the acidity number due to the formation of acids, mainly formic and acetic.[94] Thus, an antioxidant additive must delay these fuel aging processes, guaranteeing them a longer shelf-life under ideal conditions of use. The S10 B15 blend was produced from reference biodiesel-free diesel (fuel type applied on standard emission tests), which normally shows a better value of oxidation stability in relation to common diesel, considering this application is more rigorous. Thus, it is important to perform new tests using common diesel for blends (Table 3) and verify if it would exceed 30 hours in the presence of BCH and NCH and for additive-free samples. Normally, S10 B15 diesel prepared from common B0 diesel has lower induction period values when evaluated using the modified Rancimat method. Additional tests are required to evaluate the performance of BCH and NCH as antioxidant additives applied to diesel–biodiesel blends prepared using common diesel.

3.3. Molecular modeling analysis

The HOMO and LUMO orbitals over the BCH are similar while NCH presented differences. For BCH, the HOMO and LUMO orbitals are over the aromatic rings 2 and 3, while for NCH, the LUMO orbitals are located over aromatic rings 2 and 3, and the HOMO orbitals are located over aromatic ring 2 (Fig. 6). The HOMO orbital for both chalcones characterizes the bonding orbital, ionization potential (nucleophilic character) while the LUMO orbital represents the antibonding orbital, electron affinity (electrophilic character). The energy calculated for these

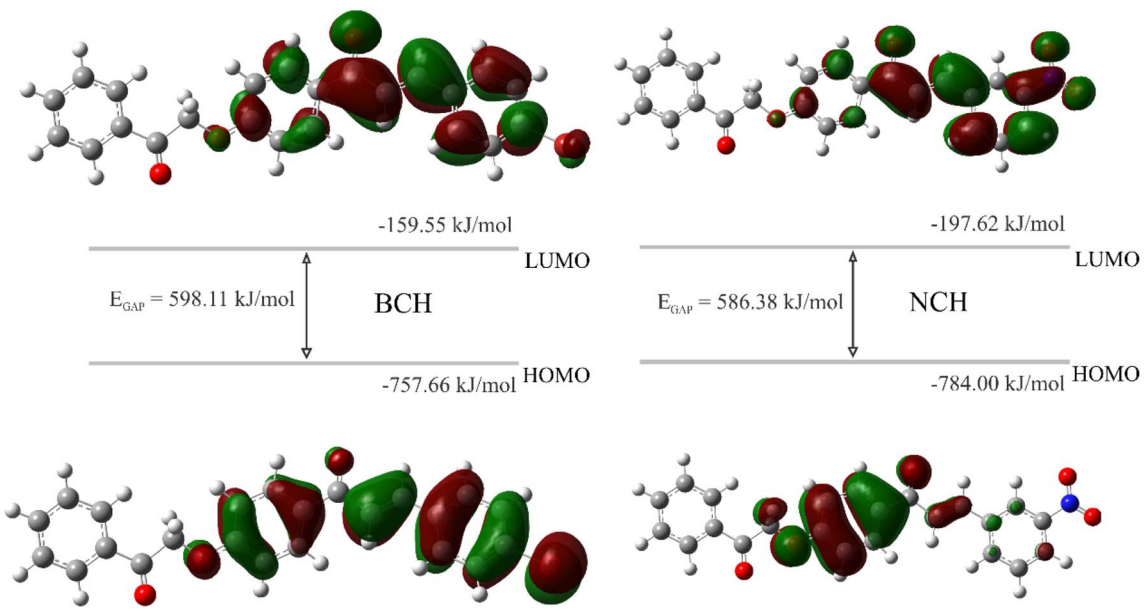

Fig. 6 Frontier molecular orbitals (HOMO/LUMO) for BCH and NCH. Orbitals calculated at M06-2X/6311++G(d, p) level of theory.

orbitals for BCH is E_{LUMO} = −159.55 kJ mol^{-1}, E_{HOMO} = −757.66 kJ mol^{-1} and E_{GAP} = 598.11 kJ mol^{-1} (E_{LUMO}–E_{HOMO}), while for NCH is E_{LUMO} = −197.62 kJ mol^{-1}, E_{HOMO} = −784.00 kJ mol^{-1} and E_{GAP} = 586.38 kJ mol^{-1}.

The high GAP energy values suggest high kinetic stability and low chemical reactivity.[95] According to these parameters, the E_{GAP} for BCH suggests greater kinetic stability than NCH. However, the values are very close. Some values of E_{GAP} for antioxidant molecules or commercial additives, such the BHT have GAP values of about 546.1 kJ mol^{-1},[96,97] toluene derivatives with GAP values of 477.8 kJ mol^{-1},[98] ether molecules with a GAP value ranging from 273.8 kJ mol^{-1} to 404.6 kJ mol^{-1},[99] thiazolidinone molecules (308.5 to 481.8 kJ mol^{-1})[100] and the *p*-phenylenediamine (56.8 kJ mol^{-1} to 114.5 kJ mol^{-1}).[101,102] The GAP values found for BCH (598.11 kJ mol^{-1}) and NCH (586.38 kJ mol^{-1}) are similar and greater than those found in the literature, indicating that both chalcones have greater kinetic stability than those already reported.

MEP (Fig. 7) was used to predict the reactivity of compounds and determine regions where nucleophilic (blue colors) and electrophilic (red colors) attacks are expected. The most electronegative zones occur in the vicinity of oxygens for the two molecules. Due to the nitro group in the NCH, additional zones of high electronegative density are generated, while the BCH presents a zone with positive electrostatic potential (+18.64 kJ mol^{-1}). Therefore, the order of decreasing electrophilic attack for the discussed compounds should be in BCH O3 (−125.68 kJ mol^{-1}) > O2 (−113.50 kJ mol^{-1}) > O1 (−112.84 kJ mol^{-1}) and in NCH O2 (−121.87 kJ mol^{-1}) > O1 (−119.69 kJ mol^{-1}) > O3 (−114.26 kJ mol^{-1}) > O4 (−110.61 kJ mol^{-1}) > O5 (−110.84 kJ mol^{-1}). In addition, regions with light blue coloration are sites with weak interaction.

To evaluate the main active sites of both molecules through an oxidative process, Fukui functions were calculated. These functions represent an important approach to explaining the reactivity in chemical systems to a radical attack.[71,72,103,104] Fig. 8 illustrates significant values (nomenclature in Fig. 1) for the selected atoms. According to Fukui's formulation,[71] higher values are associated with a higher probability of radical attack (f_{NBO}). In this study, the carbon attached to the bromine atom C_{21} in BCH has a Fukui index of 0.055, while the carbon attached to the nitro group C_{20} in NCH has a Fukui index of 0.035, indicating that the reactivity of the NCH is lower in an oxidative process, which is consistent with the data obtained experimentally.

The reaction rate constant is the most important parameter to reveal the efficiency of the degradation of a compound; in this sense, the oxidative degradation rates by the hydroxyl radical attack of BCH, NCH, diesel (represented by $C_{10}H_{20}$ molecule), and biodiesel (represented by $C_{17}H_{35}COOCH_3$ fatty acid methyl ester) compounds were calculated using a web application based on machine learning models, pySiRC,[74] whose values are 7.15 × 10^9 M^{-1} s^{-1}, 6.01 × 10^9 M^{-1} s^{-1}, 6.20 × 10^9 M^{-1} s^{-1}, and 4.98 × 10^9 M^{-1} s^{-1}, respectively. These values suggest that oxidative degradation in BCH has a higher

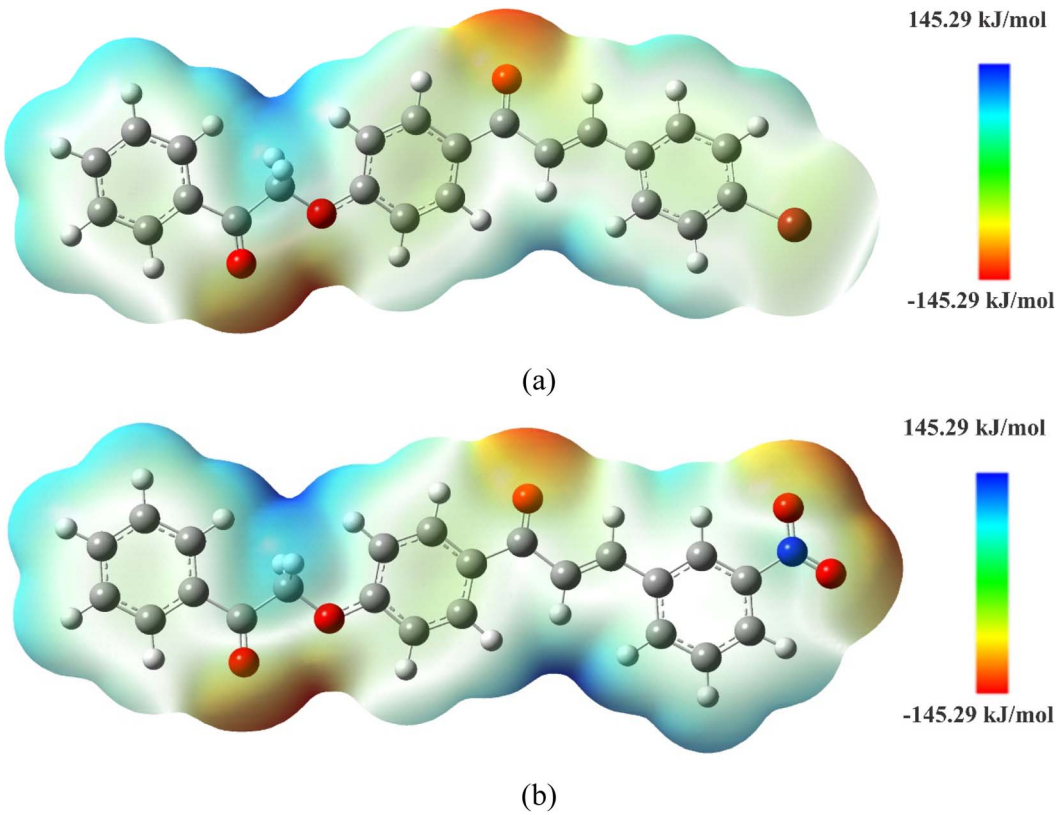

Fig. 7 MEP map for (a) BCH and (b) NCH. The density isovalue of $\rho(r)$ = 4.0 × 10^{-4} electrons per bohr^{3}contour encompassing the molecule.

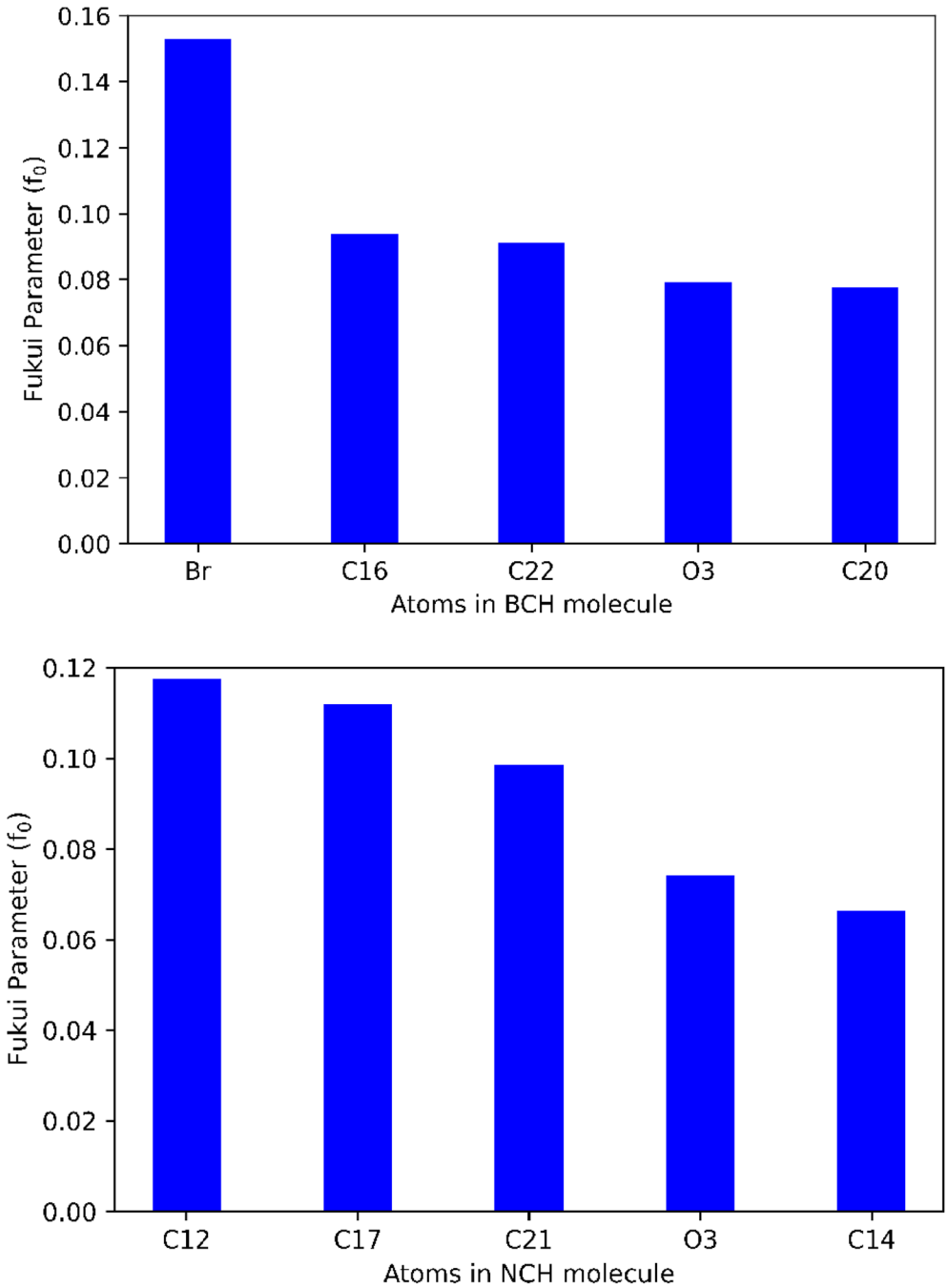

Fig. 8 Fukui function values for the radical attack on selected atoms of both molecules (see nomenclature in Fig. 1).

oxidation potential than in NCH, which is consistent with the results obtained experimentally by the modified Rancimat method. Thus, the additive is first "sacrificed" so that the later degradation occurs later in the biodiesel, indicating greater oxidative stability of the biodiesel.

4. Conclusions

The structural analysis of the compounds associated with the evaluation of their physicochemical properties provides important information that contributes to the discovery of new compounds with potential technological applications, including their use as additives for biodiesel blends, considering also that the structural conformation directly affects the chemical and reactional characteristics of a molecule. In this work, it was verified that the change of the components linked to the aromatic ring 3 of both chalcones promoted important structural changes, including that from the conformation of the crystals obtained to the reaction characteristics. Also, it indicates that the application of additives in diesel–biodiesel blends is important for preserving fuel characteristics.

The oxidative stability test for fuel + chalcones indicated that the performance of NCH even at lower concentrations (109.0 ppm of BCH and 100.7 ppm of NCH) is more promising than BCH as an antioxidant agent in a diesel/biodiesel blend. The two compounds delayed the degradation of the biofuel, preserving its properties for 90 days of storage, without any additional processing. Complementary tests can confirm whether other desirable functions of an additive in this metric are maintained or not. Theoretical calculations show that compared to other compounds similar to additives, BCH and NCH show greater kinetic stability since the chalcones are likely to be first oxidized compared to diesel-biodiesel composition. The application of these methods paved the way for clarifying and expanding the potential of BCH and NCH compounds as antioxidant additives for diesel–biodiesel blends.

Conflicts of interest

The authors declare that they have no known competing financial interests or personal relationships that could have appeared to influence the work reported in this study.

Acknowledgements

The authors are grateful to Coordenação de Aperfeiçoamento de Pessoal de Nível Superior, Conselho Nacional de Desenvolvimento Científico e Tecnológico and Fundação de Amparo à Pesquisa de Goiás. Theoretical calculations were performed in the High-Performance Computing Center of the Universidade Estadual de Goiás, and Rancimat experiments were performed in the Research and Energy Efficiency Center (CAOA Montadora de Veículos Ltda).

References

1 A. J. Ryan and R. H. Rothman, Engineering chemistry to meet COP26 targets, *Nat. Rev. Chem.*, 2022, **6**, 1–3.
2 E. Aines, Z. Clulow, A. Neilson, E. Shuckburgh and S. Evans, *COP26 Futures We Want-UK Country Profile*, 2021.
3 M. Gürü, A. Koca, Ö. Can, C. Çınar and F. Şahin, Biodiesel production from waste chicken fat based sources and evaluation with Mg based additive in a diesel engine, *Renewable Energy*, 2010, **35**, 637–643.
4 Technology, I. E. Agency. O. of E., R&D. & (Organization), *Energy technology perspectives*, International Energy Agency, 2006.
5 T. W. Hudiburg, *et al.*, Impacts of a 32-billion-gallon bioenergy landscape on land and fossil fuel use in the US, *Nat. Energy*, 2016, **1**, 15005.
6 P. Chen, *et al.*, The heterogeneous role of energy policies in the energy transition of Asia–Pacific emerging economies, *Nat. Energy*, 2022, **7**, 588–596.
7 P. Smith, *et al.*, Essential outcomes for COP26, *Global Change Biol.*, 2022, **28**, 1–3.
8 Y. Zhang, L. Duan and H. Esmaeili, A review on biodiesel production using various heterogeneous nanocatalysts: Operation mechanisms and performances, *Biomass Bioenergy*, 2022, **158**, 106356.
9 K. Romanak and T. Dixon, CO2 storage guidelines and the science of monitoring: Achieving project success under the California Low Carbon Fuel Standard CCS Protocol and other global regulations, *Int. J. Greenhouse Gas Control*, 2022, **113**, 103523.
10 G. Iyer, *et al.*, Measuring progress from nationally determined contributions to mid-century strategies, *Nat. Clim. Change*, 2017, **7**, 871–874.
11 M. Lennan and E. Morgera, The Glasgow Climate Conference (COP26), *Int. J. Mar. Coast. Law*, 2022, **37**, 137–151.
12 V. Masson-Delmotte *et al.*, IPCC, 2018: Global Warming of 1.5 C. An IPCC Special Report on the impacts of global warming of 1.5 C above pre-industrial levels and related global greenhouse gas emission pathways, in the context of strengthening the global response to the threat of climate change, sustainable development, and efforts to eradicate poverty, *Sustainable Development, and Efforts to Eradicate Poverty*, 2018.
13 S. Whitmee, R. Green, J. Phumaphi, H. Clark and A. Haines, Bridging the evidence gap to achieve a healthy, net zero future, *Lancet*, 2021, **398**, 1551–1553.
14 N. N. A. N. Yusuf, S. K. Kamarudin and Z. Yaakub, Overview on the current trends in biodiesel production, *Energy Convers. Manage.*, 2011, **52**, 2741–2751.
15 A. S. Nizami, *et al.*, Waste biorefineries: Enabling circular economies in developing countries, *Bioresour. Technol.*, 2017, **241**, 1101–1117.
16 B. Karpanai Selvan, *et al.*, Utilization of biodiesel blended fuel in a diesel engine – Combustion engine performance and emission characteristics study, *Fuel*, 2022, **311**, 122621.
17 H. Hosseinzadeh-Bandbafha, *et al.*, Biodiesel antioxidants and their impact on the behavior of diesel engines: A comprehensive review, *Fuel Process. Technol.*, 2022, **232**, 107264.
18 M. A. Hazrat, *et al.*, Techniques to improve the stability of biodiesel: a review, *Environ. Chem. Lett.*, 2021, **19**, 2209–2236.
19 F. Sundus, M. A. Fazal and H. H. Masjuki, Tribology with biodiesel: A study on enhancing biodiesel stability and its fuel properties, *Renewable Sustainable Energy Rev.*, 2017, **70**, 399–412.
20 D. Chandran, *et al.*, Critical relationship between biodiesel fuel properties and degradation of fuel delivery materials of a diesel engine, *Therm. Sci. Eng. Prog.*, 2018, **7**, 20–26.
21 Y. Palani, C. Devarajan, D. Manickam and S. Thanikodi, Performance and emission characteristics of biodiesel-blend in diesel engine: A review, *Environ. Eng. Res.*, 2020, **27**, 200338.
22 D. Singh, *et al.*, A review on feedstocks, production processes, and yield for different generations of biodiesel, *Fuel*, 2020, **262**, 116553.
23 H. Li, *et al.*, Effects of biodiesel blends on the kinetic and thermodynamic parameters of fossil diesel during

thermal degradation, *Energy Convers. Manage.*, 2019, **198**, 111930.
24 E. Symoniuk, K. Ratusz and K. Krygier, Comparison of the oxidative stability of linseed (Linum usitatissimum L.) oil by pressure differential scanning calorimetry and Rancimat measurements, *J. Food Sci. Technol.*, 2016, **53**, 3986–3995.
25 F. O. Sanches-Neto, N. D. Coutinho, F. Palazzetti and V. H. Carvalho-Silva, Temperature dependence of rate constants for the H(D) + CH4 reaction in gas and aqueous phase: deformed Transition-State Theory study including quantum tunneling and diffusion effects, *Struct. Chem.*, 2020, **31**, 609–617.
26 J. Xin, H. Imahara and S. Saka, Kinetics on the oxidation of biodiesel stabilized with antioxidant, *Fuel*, 2009, **88**, 282–286.
27 I. M. Rizwanul Fattah, H. H. Masjuki, M. A. Kalam, M. Mofijur and M. J. Abedin, Effect of antioxidant on the performance and emission characteristics of a diesel engine fueled with palm biodiesel blends, *Energy Convers. Manage.*, 2014, **79**, 265–272.
28 C. A. Moreira, *et al.*, Structural insights and antioxidant analysis of a tri-methoxy chalcone with potential as a diesel-biodiesel blend additive, *Fuel Process. Technol.*, 2022, **227**, 107122.
29 E. C. M. Faria, *et al.*, Comparative Study of Chalcones and Their Potential as Additives for Biofuels, *Energy Fuels*, 2021, **35**, 552–560.
30 G. Hou, X. Yuan, Y. Li, G. Hou and X. C. Liu, a natural chalcone, reduces 5-fluorouracil resistance of gastric cancer cells through targeting Wnt/β-catenin signal pathway, *Invest. New Drugs*, 2020, **38**, 329–339.
31 W. Eden, D. Alighiri, N. Wijayati and S. Mursiti, Synthesis of Chalcone Derivative from Clove Leaf Waste as a Natural Antioxidant, *Pharm. Chem. J.*, 2021, **55**, 269–274.
32 A. Rammohan, J. S. Reddy, G. Sravya, C. N. Rao and G. V. Zyryanov, Chalcone synthesis, properties and medicinal applications: a review, *Environ. Chem. Lett.*, 2020, **18**, 433–458.
33 S. Farooq and Z. Ngaini, Recent Synthetic Methodologies for Chalcone Synthesis (2013-2018), *Curr. Organocatal.*, 2019, **6**, 184–192.
34 S. Verma, A. Srivastava and O. Pandey, A Review on Chalcones Synthesis and their Biological Activity, *PharmaTutor*, 2018, **2**, 22–39.
35 M. Xu, P. Wu, F. Shen, J. Ji and K. Rakesh, Chalcone derivatives and their antibacterial activities: Current development, *Bioorg. Chem.*, 2019, **91**, 103133.
36 W. Dan and J. Dai, Recent developments of chalcones as potential antibacterial agents in medicinal chemistry, *Eur. J. Med. Chem.*, 2020, **187**, 111980.
37 Y. Wang, *et al.*, Synthesis and antibacterial activity of novel chalcone derivatives bearing a coumarin moiety, *Chem. Pap.*, 2019, **73**, 2493–2500.
38 M. Mellado, *et al.*, Design, synthesis, antifungal activity, and structure–activity relationship studies of chalcones and hybrid dihydrochromane–chalcones, *Mol. Diversity*, 2020, **24**, 603–615.
39 Y. Jin, Recent advances in natural antifungal flavonoids and their derivatives, *Bioorg. Med. Chem. Lett.*, 2019, **29**, 126589.
40 K. Goyal, R. Kaur, A. Goyal and R. C. Awasthi, A review on synthesis and pharmacological activities, *J. Appl. Pharm. Sci.*, 2021, **11**, 1–14.
41 S. Lahsasni, F. Korbi and N. Aljaber, synthesis, characterization and evaluation of antioxidant activities of some novel chalcones analogues, *Chem. Cent. J.*, 2014, **8**, 1–10.
42 C. Zhuang, *et al.*, Chalcone: A Privileged Structure in Medicinal Chemistry, *Chem. Rev.*, 2017, **117**, 7762–7810.
43 O. Serifi, *et al.*, Antioxidant behaviour of 2′-hydroxy-chalcones: a study of their electrochemical properties, *J. Phys. Org. Chem.*, 2013, **26**, 226–231.
44 B. Mathew, *et al.*, Anti-oxidant behavior of functionalized chalcone-a combined quantum chemical and crystallographic structural investigation, *J. Mol. Struct.*, 2017, **1146**, 301–308.
45 N. A. Shakil, M. K. Singh, M. Sathiyendiran, J. Kumar and J. C. Padaria, Microwave synthesis, characterization and bio-efficacy evaluation of novel chalcone based 6-carbethoxy-2-cyclohexen-1-one and 2H-indazol-3-ol derivatives, *Eur. J. Med. Chem.*, 2013, **59**, 120–131.
46 N. Cotelle, P. Hapiot, J. Pinson, C. Rolando and H. Vézin, Polyphenols Deriving from Chalcones: Investigations of Redox Activities, *J. Phys. Chem. B*, 2005, **109**, 23720–23729.
47 B. P. Bandgar, S. S. Gawande, R. G. Bodade, N. M. Gawande and C. N. Khobragade, Synthesis and biological evaluation of a novel series of pyrazole chalcones as anti-inflammatory, antioxidant and antimicrobial agents, *Bioorg. Med. Chem.*, 2009, **17**, 8168–8173.
48 L. O. Sallum, *et al.*, Cyclohexanone-Based Chalcones as Alternatives for Fuel Additives, *ACS Omega*, 2022, **7**, 11871–11886.
49 K. Burke, Perspective on density functional theory, *J. Chem. Phys.*, 2012, **15**, 150901.
50 G. H. Grant, W. G. Richards and G. William, *Computational chemistry*, Oxford University Primers, 1996.
51 D. H. Pereira, F. A. La Porta, R. T. Santiago, D. R. Garcia and T. C. Ramalho, New Perspectives on the Role of Frontier Molecular Orbitals in the Study of Chemical Reactivity: A Review, *Revista Virtual de Química*, 2016, **8**, 425–453.
52 M. A. Spackman and D. Jayatilaka, Hirshfeld surface analysis, *CrystEngComm*, 2009, **11**, 19–32.
53 J. Pullen and K. Saeed, Experimental study of the factors affecting the oxidation stability of biodiesel FAME fuels, *Fuel Process. Technol.*, 2014, **125**, 223–235.
54 Y. Duan, Y. Wang and D. Li, A Facile Approach for Synthesis of Benzofuro[2,3-c]Pyridines via Intramolecular Cascade Annulations, *Chin. J. Chem.*, 2014, **32**, 1103–1106.
55 G. M. Sheldrick, SHELXT – Integrated space-group and crystal-structure determination, *Acta Crystallogr., Sect. A: Found. Adv.*, 2015, **71**, 3–8.
56 G. M. Sheldrick, Crystal structure refinement with SHELXL, *Acta Crystallogr., Sect. C*, 2015, **71**, 3–8.

57 O. V. Dolomanov, L. J. Bourhis, R. J. Gildea, J. A. K. Howard and H. J. Puschmann, OLEX2: a complete structure solution, refinement and general all round good thing Olex2, *J. Appl. Crystallogr.*, 2009, **42**, 339–341.
58 C. F. Macrae, *et al.*, Mercury : visualization and analysis of crystal structures, *J. Appl. Crystallogr.*, 2006, **39**, 453–457.
59 A. L. Spek, Single-crystal structure validation with the program PLATON, *J. Appl. Crystallogr.*, 2003, **36**, 7–13.
60 C. R. Groom, I. J. Bruno, M. P. Lightfoot and S. C. Ward, The Cambridge structural database, *Acta Crystallogr., Sect. B: Struct. Sci., Cryst. Eng. Mater.*, 2016, **72**, 171–179.
61 J. J. McKinnon, M. A. Spackman and A. S. Mitchell, Novel tools for visualizing and exploring intermolecular interactions in molecular crystals, *Acta Crystallogr., Sect. B*, 2004, **60**, 627–668.
62 ANP - Site of the National Agency for Petroleum, *Natural Gas and Biofuels*, ANP Resolution No. 764.
63 *BS EN 15751-14: Automotive Fuels – Fatty acid Methyl Ester (FAME) Fuel and Blends with Diesel Fuel – Determination of Oxidation Stability by Accelerated Oxidation Method*, 2014, vol. 22.
64 X. Li, *et al.*, Oxidation degree of soybean oil at induction time point under Rancimat test condition: Theoretical derivation and experimental observation, *Food Res. Int.*, 2019, **120**, 756–762.
65 J. Zhou, Y. Xiong and X. Liu, Evaluation of the oxidation stability of biodiesel stabilized with antioxidants using the Rancimat and PDSC methods, *Fuel*, 2017, **188**, 61–68.
66 M. Frisch, G. Trucks, H. B. Schlegel, G. Scuseria, M. Robb, J. Cheeseman, G. Scalmani, V. Barone, B. Mennucci and G. Petersson, *Gaussian 09, Revision A. 02*, Gaussian Inc., Wallingford, CT, 2009, p. 200.
67 Y. Zhao and D. G. Truhlar, The M06 suite of density functionals for main group thermochemistry, thermochemical kinetics, noncovalent interactions, excited states, and transition elements: Two new functionals and systematic testing of four M06-class functionals and 12 other function, *Theor. Chem. Acc.*, 2008, **120**, 215–241.
68 R. Krishnan, J. S. Binkley, R. Seeger and J. A. Pople, Self-consistent molecular orbital methods. XX. A basis set for correlated wave functions, *J. Chem. Phys.*, 1980, **72**, 650–654.
69 A. D. McLean and G. S. Chandler, Contracted Gaussian basis sets for molecular calculations. I. Second row atoms, Z=11–18, *J. Chem. Phys.*, 1980, **72**, 5639–5648.
70 P. Sjoberg and P. Politzer, Use of the Electrostatic Potential at the Molecular Surface, *J. Phys. Chem.*, 1990, **94**, 3959–3961.
71 P. López and F. Méndez, Fukui function as a descriptor of the imidazolium protonated cation resonance hybrid structure, *Org. Lett.*, 2004, **6**, 1781–1783.
72 J. Melin, P. W. Ayers and J. V. Ortiz, Removing electrons can increase the electron density: a computational study of negative Fukui functions, *J. Phys. Chem. A*, 2007, **111**, 10017–10019.
73 T. Lu and F. Chen, Multiwfn: A multifunctional wavefunction analyzer, *J. Comput. Chem.*, 2012, **33**, 580–592.
74 F. O. Sanches-Neto, J. R. D. S, L. H. K. Q. Junior and V. H. Carvalho-Silva, 'pySiR. C. ': Machine learning combined with molecular fingerprints to predict the reaction rate constant of the radical-based oxidation processes of aqueous organic contaminants, *Environ. Sci. Technol.*, 2021, **55**, 12437–12448.
75 L. J. Farrugia, ORTEP-3 for Windows-a version of ORTEP-III with a Graphical User Interface (GUI), *J. Appl. Crystallogr.*, 1997, **30**, 565.
76 S. J. K. Pond, *et al.*, One- and Two-Photon Spectroscopy of Donor–Acceptor–Donor Distyrylbenzene Derivatives: Effect of Cyano Substitution and Distortion from Planarity, *J. Phys. Chem. A*, 2002, **106**, 11470–11480.
77 P. P. Firmino, *et al.*, Synthesis, Molecular Structure, Thermal and Spectroscopic Analysis of a Novel Bromochalcone Derivative with Larvicidal Activity, *Crystals*, 2022, **12**, 440.
78 K. Jomová, *et al.*, A Switch between Antioxidant and Prooxidant Properties of the Phenolic Compounds Myricetin, Morin, 3′,4′-Dihydroxyflavone, Taxifolin and 4-Hydroxy-Coumarin in the Presence of Copper(II) Ions: A Spectroscopic, Absorption Titration and DNA Damage Study, *Molecules*, 2019, **24**, 4335.
79 S. N. López, *et al.*, vitro antifungal evaluation and structure–activity relationships of a new series of chalcone derivatives and synthetic analogues, with inhibitory properties against polymers of the fungal cell wall, *Bioorg. Med. Chem.*, 2001, **9**, 1999–2013.
80 Z. Nowakowska, A review of anti-infective and anti-inflammatory chalcones, *Eur. J. Med. Chem.*, 2007, **42**, 125–137.
81 D. Gupta and D. Jain, Chalcone derivatives as potential antifungal agents: Synthesis, and antifungal activity, *J. Adv. Pharm. Technol. Res.*, 2015, **6**, 114.
82 M. Leopoldini, T. Marino, N. Russo and M. Toscano, Antioxidant Properties of Phenolic Compounds: H-Atom versus Electron Transfer Mechanism, *J. Phys. Chem. A*, 2004, **108**, 4916–4922.
83 I. Lawan, *et al.*, Synthesis, properties and effects of a multi-functional biodiesel fuel additive, *Fuel Process. Technol.*, 2020, **198**, 106228.
84 R. K. Saluja, V. Kumar and R. Sham, Stability of biodiesel – A review, *Renewable Sustainable Energy Rev.*, 2016, **62**, 866–881.
85 ANP - Site of the National Agency for Petroleum, Natural Gas and Biofuels, ANP Resolution No. 798/2019, available in: **https://www.gov.br/anp/pt-br/assuntos/producao-e-fornecimento-de-biocombustiveis/biodiesel/especificacao-do-biodiesel**.
86 British Standards Institution, *BS EN 590:2013 Automotive fuels Diesel Requirements and test methods*, BSI, 2013.
87 G. Joshi, B. Y. Lamba, D. S. Rawat, S. Mallick and K. S. R. Murthy, Evaluation of Additive Effects on Oxidation Stability of Jatropha Curcas Biodiesel Blends

with Conventional Diesel Sold at Retail Outlets, *Ind. Eng. Chem. Res.*, 2013, **52**, 7586–7592.

88 I. M. Rizwanul Fattah, *et al.*, Experimental investigation of performance and regulated emissions of a diesel engine with Calophyllum inophyllum biodiesel blends accompanied by oxidation inhibitors, *Energy Convers. Manage.*, 2014, **83**, 232–240.

89 A. K. Agarwal, D. Khurana and A. Dhar, Improving oxidation stability of biodiesels derived from Karanja, Neem and Jatropha: step forward in the direction of commercialisation, *J. Cleaner Prod.*, 2015, **107**, 646–652.

90 W. W. Focke, I. van der Westhuizen and X. Oosthuysen, Biodiesel oxidative stability from Rancimat data, *Thermochim. Acta*, 2016, **633**, 116–121.

91 S. Nogales-Delgado, A. Guiberteau and J. M. Encinar, Effect of tert-butylhydroquinone on biodiesel properties during extreme oxidation conditions, *Fuel*, 2022, **310**, 122339.

92 K. Varatharajan and D. S. Pushparani, Screening of antioxidant additives for biodiesel fuels, *Renewable Sustainable Energy Rev.*, 2018, **82**, 2017–2028.

93 G. Karavalakis, D. Karonis and S. Stournas, Evaluation of the Oxidation Stability of Diesel/Biodiesel Blends using the Modified Rancimat Method, *SAE Int. J. Fuels Lubr.*, 2009, **2**, 839–849.

94 C. Romola, *et al.*, A comprehensive review of the selection of natural and synthetic antioxidants to enhance the oxidative stability of biodiesel, *Renewable Sustainable Energy Rev.*, 2021, **145**, 111109.

95 G. Zhang and C. B. Musgrave, Comparison of DFT Methods for Molecular Orbital Eigenvalue Calculations, *J. Phys. Chem. A*, 2007, **111**, 1554–1561.

96 P. Chinna Babu, N. Sundaraganesan, Ö. Dereli and E. F. T.-I. R. Türkkan, FT-Raman spectra, density functional computations of the vibrational spectra and molecular geometry of butylated hydroxy toluene, *Spectrochim. Acta, Part A*, 2011, **79**, 562–569.

97 R. Raja, S. Seshadri, T. Gnanasambandan and R. R. Saravanan, Crystal growth and properties of NLO optical crystal – Butylated Hydroxy Toluene (BHT), *Spectrochim. Acta, Part A*, 2015, **138**, 13–20.

98 V. Krishna Kumar, S. Suganya and R. Mathammal, Molecular structure, vibrational spectra, HOMO, LUMO and NMR studies of 2,3,4,5,6-Penta Bromo Toluene and Bromo Durene based on density functional calculations, *Spectrochim. Acta, Part A*, 2014, **125**, 201–210.

99 A. S. Rad, Al-doped graphene as modified nanostructure sensor for some ether molecules: Ab-initio study, *Synth. Met.*, 2015, **209**, 419–425.

100 H. Mohammed, S. Attia, M. Nessim, M. Shaaban and A. El-Bassoussi, Studies on Some Thiazolidinones as Antioxidants for Local Base Oil, *Egypt. J. Chem.*, 2019, **62**, 1219–1234.

101 M. A. Diab, A. Z. El-Sonbati, N. A. El-Ghamaz, Sh. M. Morgan and O. El-Shahat, Conducting polymers X: Dielectric constant, conduction mechanism and correlation between theoretical parameters and electrical conductivity of poly (*N*,*N*′-bis-sulphinyl p-phenylenediamine-2,6-diaminopyridine) and poly (*N*,*N*′-bis-sulphinyl p-phenylenediamine, *Eur. Polym. J.*, 2019, **115**, 268–281.

102 S. Yang, C. Ye, X. Song, L. He and F. Liao, Theoretical calculation based synthesis of a poly(p-phenylenediamine)–Fe 3 O 4 composite: a magnetically recyclable photocatalyst with high selectivity for acid dyes, *RSC Adv.*, 2014, **4**, 54810–54818.

103 D. A. Milenković, *et al.*, Advanced oxidation process of coumarins by hydroxyl radical: Towards the new mechanism leading to less toxic products, *Chem. Eng. J.*, 2020, **395**, 124971.

104 F. O. Sanches-Neto, B. Ramos, A. M. Lastre-acosta, A. C. S. C. Teixeira and V. H. Carvalho-Silva, Aqueous Picloram Degradation by Hydroxyl Radicals: Unveiling Mechanism, Kinetics, and Ecotoxicity through Experimental and Theoretical Approaches, *Chemosphere*, 2021, 130401, DOI: **10.1016/j.chemosphere.2021.130401**.